Received: 10 November 2024 | Revised: 14 April 2025 | Accepted: 7 June 2025

DOI: 10.33012/navi.710

REGULAR PAPERS

Single-Satellite Lunar Navigation via Doppler Shift Observables for the NASA Endurance Mission

Kaila M. Y. Coimbra[1] | **Marta Cortinovis**[1] | **Tara Mina**[2] | **Grace Gao***[1]

[1] Department of Aeronautics and Astronautics, Stanford University

[2] Daniel Guggenheim School of Aerospace Engineering, Georgia Institute of Technology

Correspondence
*Grace Gao
Department of Aeronautics and Astronautics, Stanford University
Stanford, CA, USA 94305
Email: gracegao@stanford.edu

Abstract

The National Aeronautics and Space Administration (NASA) Endurance rover mission concept is designed to enable the exploration and collection of samples along a 2000-km traverse within the Moon's South Pole-Aitken (SPA) impact basin. Precise geotagging of these samples will be critical to the mission's scientific objectives, which include characterizing the Solar System's chronology and the Moon's geological evolution. Concurrently, the European Space Agency (ESA) and Surrey Satellite Technology Ltd. (SSTL) are partnering to launch the Lunar Pathfinder satellite to provide communication services to lunar surface users, including the NASA Endurance rover. To enable precise absolute localization of the rover throughout its 2000-km traverse, we have investigated the achievable position estimation by opportunistically leveraging the Doppler shift observables from the Lunar Pathfinder's downlink communication signals with no navigation payload.

With only one satellite available, we accumulated Doppler shift measurements over time while the rover was stationary and refined the rover's position estimate through a weighted batch filter framework. Through simulations, we modeled the effects of Doppler shift measurement uncertainty, which includes the frequency error of the rover clock as well as errors due to carrier tracking as a function of the carrier-to-noise ratio C/N_0. The state estimation performance is evaluated at different key locations of the SPA basin under varying degrees of satellite ephemeris uncertainty and clock stability. With this framework of using the Doppler shift as the only navigation observable, we find that the Lunar Pathfinder is able to opportunistically localize the Endurance rover with sub-10-m accuracy, on average, within two orbital periods of the Lunar Pathfinder. To the best of the authors' knowledge, this paper is the first to examine the achievable localization of a lunar surface asset using only a single satellite that is not equipped with a navigation payload.

Keywords

Doppler shift, lunar navigation, Lunar Pathfinder, NASA Endurance mission, signals of opportunity

1 | INTRODUCTION

The National Aeronautics and Space Administration (NASA) is actively working toward establishing a permanent human presence on the Moon and in cislunar space through the Artemis program (NASA, 2022b). To facilitate eventual human exploration and long-term stay, NASA and other entities have been developing autonomous exploratory rover missions to study the lunar South Pole. One of these mission concepts is Endurance, a long-range lunar rover that aims to collect and return surface samples from the South Pole-Aitken (SPA) impact basin (Keane et al., 2022). These samples will provide key insights into the Solar System's chronology and characterize the geologic diversity of the largest and oldest impact basin on the Moon. The Endurance rover will collect these samples from key waypoints distributed across its planned 2000-km-long traverse.

1.1 | Related Works

To properly geotag the collected samples, precise absolute localization of the rover is critical. For most planetary rover missions, including Endurance, the global localization error requirement is 10 m (Cauligi et al., 2023). Currently, the NASA Jet Propulsion Laboratory has proposed two vision-based techniques for localization: LunarNav and ShadowNav. LunarNav involves autonomous crater detection using onboard cameras and matching of the craters to a developed database of lunar features that are mapped from satellite imagery (Daftry et al., 2023). For the scenario in which Endurance is not in a sunlit area, ShadowNav detects shadows from crater edges and matches the shadows to an onboard map (Cauligi et al., 2023). Although the positioning errors for both techniques are within the localization error requirement of 10 m, both methods are computationally expensive and memory-intensive, as they require Endurance to autonomously run visual matching algorithms as well as store the maps onboard. Furthermore, the positioning accuracy of these methods is highly dependent on the quality of the maps' resolution.

Satellite-based localization strategies have also been investigated for lunar surface applications. Prior works have shown that weak terrestrial Global Positioning System (GPS) signals reaching cislunar space can be utilized for absolute positioning on the lunar surface (Iiyama et al., 2023). However, given that the SPA impact basin is on the far side of the Moon, GPS sidelobe signals will not be accessible to the Endurance rover during its mission (Keane et al., 2022). Other works have investigated using a joint Doppler and ranging approach, achieving sub-10-m-level positioning accuracies with two lunar satellites (Jun et al., 2022, 2023). Another study has explored using a single lunar satellite to localize a ground user via a law-of-cosines scheme (Cheung et al., 2019). Although these localization approaches use few satellites, they require a lunar reference station within 10–15 km of the user, which is not feasible for the 2000-km traverse planned for Endurance.

Cortinovis et al. (2024) assessed the achievable localization accuracy of the Endurance rover using only a single satellite, the Lunar Pathfinder satellite, assuming that it is equipped with a radiometric navigation payload. The two-way ranging method proposed by Cortinovis et al. (2024) was successful in achieving sub-10-m-level positioning accuracy within 4 h. However, in the time frame of the Endurance mission, it is likely that the Lunar Pathfinder will not have a navigation payload to provide ranging observables and will only provide communication services for lunar surface users (SSTL, 2022). These constraints on the mission

scenario have motivated this work to investigate the use of already available downlink communication signals to opportunistically extract navigation observables. In this paper, we investigate a framework to provide absolute localization for the Endurance rover using Doppler shift observables from a single satellite that is not equipped with a navigation payload.

Prior navigation systems that employed Doppler shift measurements include TRANSIT, the first satellite navigation system ever implemented. TRANSIT was conceptualized in the late 1950s and became operational in the mid-1960s. Because of the low number of satellites that were deployed for TRANSIT, the system was primarily intended to update the position of resurfaced submarines that were stationary for hours or days at a time. TRANSIT was able to localize within 5 m for three-dimensional (3D) positioning accuracy if the receiver was stationary for several days (Misra & Enge, 2010). More recently, methods that exploit signals of opportunity from large low Earth orbit (LEO) constellations have been of interest to the navigation community. In his paper aptly subtitled "TRANSIT on steroids," Psiaki (2021) reported that large LEO constellations, such as OneWeb, Starlink, and Kuiper, will not have the capability to send pseudorange measurements. By utilizing the carrier Doppler shift of these downlink signals, Psiaki (2021) demonstrated that sub-5-m-level positioning accuracy can be achieved with LEO satellite constellations. This multi-satellite scenario enables the simultaneous accumulation of multiple measurements. In contrast, the single-satellite scenario presented in this paper necessitates the accumulation of measurements over time to ensure sufficient geometric diversity in the measurements, much like the original TRANSIT system's mode of operation. The TRANSIT navigation system assumes that the clock onboard the satellite and user is stable enough that the clock drift is constant over the measurement window (Kershner & Newton, 1962). In this paper, we also assume that the rover clock drift is constant over the measurement window and that the satellite clock is stable.

1.2 | Proposed Approach

In this work, we leverage the communication signal from the Lunar Pathfinder to localize the Endurance rover. We assume that the rover remains stationary while obtaining a positioning fix and that it is equipped with a clock that has a constant drift over the measurement window. A flow chart of the high-level approach proposed in this paper is shown in Figure 1.

Given the specifications of the satellite's communication signal (SSTL, 2022), we simulate Doppler shift measurements received by the Endurance rover at key waypoints along the rover's path. For localization, we accumulate these Doppler measurements over time, which the receiver is able to obtain using a phase locked loop (PLL). The Doppler shift measurement model takes into account uncertainty from ephemeris errors, the rover's clock stability, and the receiver's carrier tracking loop errors. Then, we solve for the rover position using a weighted batch filter algorithm of the accumulated Doppler measurements.

In this analysis, we simulate the Lunar Pathfinder satellite in an elliptical lunar frozen orbit (ELFO). The noise for the Doppler shift measurements is modeled as a function of the carrier-to-noise ratio, obtained by modeling the transmitter and receiver antenna gain patterns. We also account for the frequency error of the rover clock in the measurement model. To provide absolute localization for the Endurance rover, our approach estimates the mean and the 99th percentile (99%) of the absolute positioning error across 100 Monte Carlo realizations. We

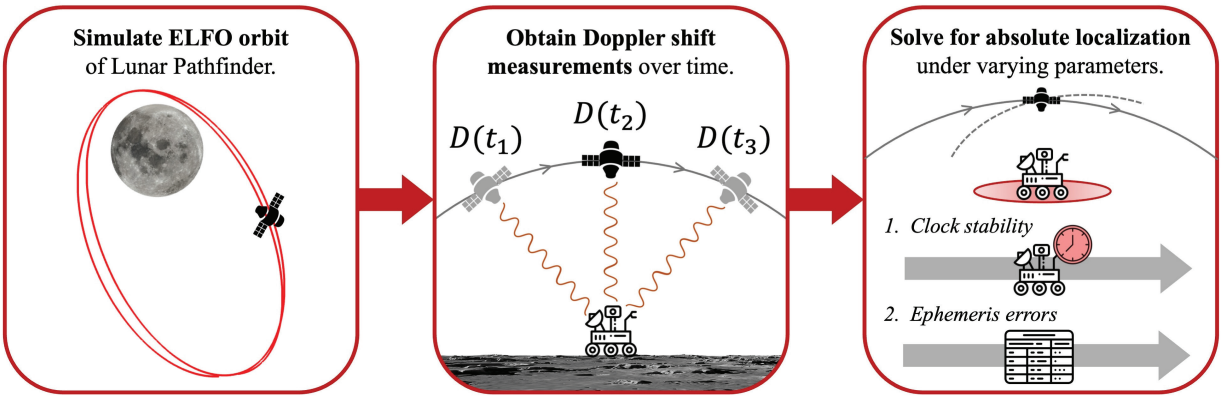

FIGURE 1 Flow chart of the proposed approach
First, we simulate the orbital trajectory of the Lunar Pathfinder. Then, we obtain Doppler shift measurements that the Endurance rover will receive over time. Finally, we perform batch filter optimization to solve for the rover's absolute localization under different degrees of clock stability and ephemeris errors.

investigate these performance metrics under different degrees of clock stability and satellite ephemeris errors.

1.3 | Key Contributions

A description of the new and innovative aspects of this paper is given below. This work was also presented as a conference paper at the Institute of Navigation GNSS+ conference in September 2024 (Coimbra et al., 2024):

- To the best of the authors' knowledge, this paper is the first to analyze the achievable localization accuracy of a lunar surface user relying solely on Doppler shift measurements from a single satellite without a dedicated navigation payload.
- We formulate a Doppler measurement error model to simulate realistic measurements from the Lunar Pathfinder communication signal, which accounts for effects including satellite ephemeris uncertainty, signal link budget, carrier tracking loop errors, and rover clock drift.
- Through Monte Carlo simulations, this work compares the trend in positioning errors over time when the rover is placed at different locations on the Moon.
- We perform sensitivity analyses on the convergence time to achieve sub-10-m-level positioning under various degrees of clock stability and ephemeris error uncertainty.

1.4 | Paper Organization

This paper is organized as follows: Section 2 outlines how the scenario is modeled, including Doppler shift measurement generation, the satellite orbit, transmitter and receiver antenna parameters, and PLL tracking error modeling. Section 3 describes the state estimation framework that refines the rover's position estimate from the Doppler shift observables. Section 4 details the simulation set-up, and Section 5 provides a discussion of the results. Finally, Section 6

provides an overview of the accomplished tasks and summarizes the main findings of the paper.

2 | SCENARIO MODELING

In this section, we discuss how we model the scenario presented in this paper, including the Doppler shift observables obtained from the Lunar Pathfinder, the satellite orbit, and the communication signal transmitted from the satellite to the rover. We also detail the error models implemented in this work for satellite ephemeris and pseudorange rate measurements.

2.1 | Generation of Doppler Shift Measurements

Constrained to a single communication satellite, the Lunar Pathfinder, we utilize Doppler shift measurements as the observable for state estimation. Doppler shift measurements D are obtained by calculating the difference between the frequency of the signal emitted at the source f_{source} and the frequency of the signal received by the rover f_{received} due to relative motion between the satellite and the rover. Given that the Lunar Pathfinder satellite has not yet been launched into lunar orbit, in this work, we must simulate the Doppler shift measurements that are observed by the rover. In particular, the Doppler shift can be modeled as follows:

$$D^{(t)} = f_{\text{received}}(t) - f_{\text{source}} = -\frac{\dot{\rho}_{\text{obs}}^{(t)} f_{\text{source}}}{c} \tag{1}$$

where $c = 299\,792\,458$ m/s is the speed of light and $\dot{\rho}_{\text{obs}}$ is the observed pseudorange rate, or the apparent rate of change in distance between the satellite and the rover.

The rover's observed pseudorange rate measurements are a function of the true range rate $\dot{\rho}_{\text{true}}$, the relative clock drift between the satellite and the rover, and a measurement error term. The observed, or noisy, pseudorange rate model is as follows:

$$\dot{\rho}_{\text{obs}}^{(t)} = \dot{\rho}_{\text{true}}^{(t)} + c\left(\dot{\delta t}_{\text{sat}} - \dot{\delta t}_{\text{rov}}\right) + \epsilon_{\dot{\rho}}^{(t)}, \quad \epsilon_{\dot{\rho}} \sim N\left(0, \sigma_{\dot{\rho}}^2\right) \tag{2}$$

where $\dot{\delta t}_{\text{sat}}$ and $\dot{\delta t}_{\text{rov}}$ are the clock drifts of the satellite and rover, respectively. The pseudorange rate measurement error term $\epsilon_{\dot{\rho}}$ is modeled as zero-mean white Gaussian noise with variance $\sigma_{\dot{\rho}}^2$, which is defined later in Section 2.5.3. The true range rate $\dot{\rho}_{\text{true}}$ is defined as the projection of the satellite velocity onto the line of sight between the rover and the satellite (Misra & Enge, 2010):

$$\dot{\rho}_{\text{true}}^{(t)} = \mathbf{v}_{\mathbf{sat}}^{(t)} \cdot \frac{\mathbf{x}_{\mathbf{sat}}^{(t)} - \mathbf{x}_{\mathbf{rov}}}{\left\| \mathbf{x}_{\mathbf{sat}}^{(t)} - \mathbf{x}_{\mathbf{rov}} \right\|}, \ \mathbf{x}^{(t)} = \begin{bmatrix} x^{(t)} & y^{(t)} & z^{(t)} \end{bmatrix}^\top, \ \mathbf{v}^{(t)} = \begin{bmatrix} \dot{x}^{(t)} & \dot{y}^{(t)} & \dot{z}^{(t)} \end{bmatrix}^\top \tag{3}$$

where $\mathbf{x}_{\mathbf{sat}}^{(t)}$ and $\mathbf{v}_{\mathbf{sat}}^{(t)}$ represent the 3D satellite position and velocity, respectively, at time t and $\mathbf{x}_{\mathbf{rov}}$ represents the stationary rover position in the Moon principal axis frame (Folta et al., 2022).

TABLE 1
The Six Keplerian Orbital Elements and Other Orbital Parameters of the Lunar Pathfinder's Trajectory (SSTL, 2022)

Orbital Parameter	Value
Semi-major axis [km]	5740
Eccentricity	0.58
Inclination [°]	54.856
Right ascension of the ascending node [°]	0
Argument of the pericenter [°]	86.322
Mean anomaly [°]	180
Periselene altitude [km]	673
Aposelene altitude [km]	7331
Orbital period [h]	10.84

In this study, we assume that the rover clock drift remains constant throughout the measurement window and that the Lunar Pathfinder carries a stable atomic clock with negligible drift over this period. Although these assumptions simplify the formulation, they also reflect the lack of publicly available data on the expected performance of the clocks onboard the Lunar Pathfinder and the Endurance rover. In reality, the satellite clock may exhibit drift over extended observation periods, and the rover clock may experience higher-order drift effects. Although these effects are not modeled in this study, future work could incorporate higher-fidelity clock models to assess their impact on the rover's state estimation as more information about the satellite and rover becomes available.

2.2 | Satellite Orbit Model

The European Space Agency (ESA) and Surrey Satellite Technology Ltd. (SSTL) have designed the Lunar Pathfinder to orbit the Moon in an ELFO with orbital elements defined in the Moon orbital plane frame of reference, as shown in Table 1 (SSTL, 2022). The orbital period is provided, as well as the periselene and aposelene altitudes. This orbital path was chosen to ensure a long duration of coverage of the Moon's southern hemisphere as well as long-term stability.

2.3 | Communication Signal Model

In this section, we discuss the structure of the Lunar Pathfinder's communication signal, the parameters of the satellite's transmitter and the rover's receiver, and the model for the carrier-to-noise density ratio C/N_0.

2.3.1 | Lunar Pathfinder Communication Signal

The Lunar Pathfinder will provide both S-band and ultra-high-frequency communication channels to lunar users. The frequency for the downlink signals is set to be between 2025 and 2110 MHz. The rover's primary communication channel with the Lunar Pathfinder will be through S-band (Keane et al., 2022); thus, we use a midpoint value of 2050 MHz for our simulations.

2.3.2 | Transmitter Antenna

Per Lunar Pathfinder's specification document (SSTL, 2022), the range of effective isotropic radiated power (EIRP) that the satellite will transmit to an autonomous rover is 12–26.5 dB W. The S-band downlink signal is specified to have a half-power beamwidth (HPBW) angle of 7.1°. Thus, in this work, we model the transmitting parabolic antenna gain pattern as having a power of 26.5 dB W at boresight, with an HPBW angle of 7.1°.

2.3.3 | Receiver Antenna and Signal Tracking Loop

To communicate with the Lunar Pathfinder, the Endurance rover will be equipped with a two-axis gimbaled 0.75-m S-band high-gain antenna (Keane et al., 2022). The Endurance rover will have an antenna gain G_r of 22.5 dB and will track the Lunar Pathfinder as it moves in the sky. Keane et al. (2022) reported that satellite tracking does not have to be very precise, as a 3° tracking error will result in only a 0.5-dB gain loss. Therefore, we apply a conservative assumption that the receiver antenna gain G_r is 22 dB, owing to tracking error.

2.3.4 | Carrier-to-Noise Density Modeling

Given the EIRP of the transmitter and the gain of the receiver antenna, we can determine the signal quality based on the received carrier-to-noise density ratio C/N_0. The C/N_0 metric defines the pseudorange rate measurement error covariance, which will be elaborated on in Section 2.5. The received C/N_0 is a function of the received isometric power P_r and the receiver's gain-to-noise-temperature ratio g/T, as follows (in dB Hz) (Delépaut et al., 2020; Misra & Enge, 2010):

$$C/N_0 = P_r + g/T - k \tag{4}$$

where k is the Boltzmann constant, which is −228.6 dBW/(K Hz). The received isometric power P_r is based on the EIRP as a function of the off-boresight angle β and the free space path loss, which is a function of the signal frequency f_S and the distance between the transmitter and the receiver r:

$$P_r = EIRP(\beta) - 20\log_{10}\left(\frac{4\pi r f_S}{c}\right) \tag{5}$$

The receiver's gain-to-noise-temperature ratio g/T takes into account losses from the system temperatures. The equivalent noise temperature T_{eq} in Kelvin is a function of the receiver's system noise temperature T_{sys} and the noise figure from the receiver's low noise amplifier (LNA) NF_{LNA}, with a reference temperature of 290 K used at the input of the LNA (Cortinovis et al., 2024; Delépaut et al., 2020). Equation (7) gives the formula for the equivalent noise temperature T_{eq} converted to its noise figure in dB. The receiver parameters in Equations (6) and (7) are listed in Table 2:

$$g/T = G_r - T_{\text{eq}} \tag{6}$$

$$T_{\text{eq}} = 10\log_{10}\left(T_{\text{sys}} + 290\left(10^{NF_{\text{LNA}}/10} - 1\right)\right) \tag{7}$$

TABLE 2
Parameters Associated with the Endurance Rover Receiver
These constants are used to obtain C/N_0 as shown in Equations (4)–(7). The system noise temperature and noise figure are values for the S-band receiver of a lunar surface rover (Audet et al., 2024).

Parameter	Symbol	Value
Gain of the receiver antenna [dB]	G_r	22.0
System noise temperature of the receiver antenna [K]	T_{sys}	113
Noise figure of the receiver LNA [dB]	NF_{LNA}	1

2.4 | Satellite Ephemeris Error Model

ESA and SSTL have not yet released the expected ephemeris errors of the Lunar Pathfinder. We assume that the rover will be able to downlink ephemeris information through the communication signal, but the frequency at which the rover will have access to the updated information and the preciseness of the ephemeris are unknown. Given that a communication satellite relies less heavily on precise ephemeris knowledge than a navigation satellite would, we can infer that the ephemeris errors cited in the Lunar Relay Services Requirements Document for lunar navigation satellites will present a lower bound, or best-case scenario (NASA, 2022a). According to the signal-in-space error (SISE) requirements for a lunar relay positioning, navigation, and timing satellite, the SISE position error is 13.43 m and the SISE velocity error is 1.2 mm/s, both at 3σ (NASA, 2022a).

In this study, we model the satellite ephemeris errors as zero-mean white Gaussian noise. While time-correlated random walks may more accurately represent the accumulation of ephemeris errors, a white noise model avoids assumptions about the satellite's ephemeris update rate and ensures that the ephemeris errors early in the measurement accumulation window are not underestimated, which is crucial for evaluating worst-case positioning performance. Because of the uncertainty in the Lunar Pathfinder's ephemeris knowledge, we conduct a sensitivity analysis on the rover's positioning error with varying degrees of satellite ephemeris error in Section 5.4. Thus, we provide the rover with erroneous satellite position and velocity states:

$$\mathbf{x}_{\mathbf{sat,noise}} = \mathbf{x}_{\mathbf{sat,true}} + \boldsymbol{\epsilon}_{\mathbf{eph,\,pos}} \tag{8}$$

$$\mathbf{v}_{\mathbf{sat,noise}} = \mathbf{v}_{\mathbf{sat,true}} + \boldsymbol{\epsilon}_{\mathbf{eph,\,vel}} \tag{9}$$

where the satellite position and velocity errors are sampled as $\boldsymbol{\epsilon}_{\mathbf{eph,pos}} \sim \mathcal{N}(0, \sigma^2_{\text{eph,pos}_{xyz}} \mathbf{I}_3)$ and $\boldsymbol{\epsilon}_{\mathbf{eph,vel}} \sim \mathcal{N}(0, \sigma^2_{\text{eph,vel}_{xyz}} \mathbf{I}_3)$ and where $\mathbf{I}_3$ represents a 3×3 identity matrix.

2.5 | Pseudorange Rate Measurement Error Model

Outside of ephemeris errors, we must account for uncertainty in the pseudorange rate measurements. In this section, we discuss how we model the noise due to carrier tracking and clock frequency errors.

TABLE 3
Parameters for PLL Tracking
These values are commonly used for PLL error modeling (Audet et al., 2024; Kaplan & Hegarty, 2017; Nardin et al., 2023).

Parameter	Symbol	Value
PLL bandwidth [Hz]	B_{PLL}	10
Coherent time integration [s]	T	0.02

2.5.1 | Carrier Tracking

For this pseudorange rate model, we assume that carrier tracking is one of the main sources of error. We predict that the receiver will track the incoming carrier frequency using a PLL. The thermal noise of the PLL is often the largest source of error in tracking the carrier frequency (Kaplan & Hegarty, 2017). The PLL thermal noise in velocity $\sigma_{\text{PLL,vel}}$ (in units of m/s) is given in Equation (10). Note that the PLL thermal noise error provided in Equation (10) is for Doppler tracking; thus, the formulation is divided by the integration time T (Borio et al., 2011; Kaplan & Hegarty, 2017). The constants used in Equation (10) are detailed in Table 3:

$$\sigma_{\text{PLL,vel}} = \frac{c}{2\pi f_S T}\sqrt{\frac{B_{\text{PLL}}}{C/N_0}\left(1+\frac{1}{2T\,C/N_0}\right)} \tag{10}$$

2.5.2 | Clock Stability

Another contributor to the measurement error is the frequency error of the rover clock. The frequency error σ_{clock} can be described by the following equations (O'Dea et al., 2019):

$$\sigma_{\text{clock}} = c \cdot \sigma_f \tag{11}$$

$$\sigma_f^2 = \frac{h_0}{2\tau} + 4h_{-1} + \frac{8}{3}\pi^2\tau h_{-2} \tag{12}$$

where σ_f is the deviation in the fractional frequency of the rover clock (Krawinkel & Schön, 2016). h_0, h_{-1}, and h_{-2} are the power spectral density (PSD) coefficients that describe the clock stability, and τ is the measurement sampling time. We only need to consider the rover clock's frequency error because the satellite clock's frequency error is encapsulated by the SISE, which is accounted for in the satellite ephemeris error model (note that the satellite's clock drift, which is distinct from its frequency error, is still included in the measurement model, as shown in Equation (2)).

In this work, we consider four rover clocks of various sizes, weights, and power consumptions (SWaP). Table 4 details the time deviation (TDEV) values per day and the PSD coefficients of the considered rover clocks with increasing SWaP. As expected, the lower-SWaP clocks have larger TDEV values per day and, therefore, a larger clock drift (note that clock drift is the TDEV per second). We investigate the performance of all four clocks in our clock sensitivity study in Section 5.3.

TABLE 4
SWaP Values, TDEV Values Per Day, and PSD Coefficients for the Rover Clock Candidates (Bhamidipati et al., 2023; Schmittberger & Scherer, 2020)
The Excelitas RAFS clock is stable enough that the contributions from the h_{-1} and h_{-2} coefficients are considered to be negligible.

Clock type	Size [cm^3]	Weight [kg]	Power [W]	TDEV per day [μs]	h_0 [s^2/s]	h_{-1} [s^2/s^2]	h_{-2} [s/s^2]
Microchip CSAC	17	0.035	0.12	1.5	1.3×10^{-20}	1.0×10^{-24}	3.7×10^{-29}
Microchip MAC	50	0.086	5	0.17	4.7×10^{-22}	1.2×10^{-25}	1.7×10^{-30}
SRS PRS 10	155	0.6	14.4	7.0×10^{-2}	1.3×10^{-22}	2.3×10^{-26}	3.3×10^{-31}
Excelitas RAFS	1645	6.35	39	4.8×10^{-3}	8.0×10^{-27}	–	–

2.5.3 | *Total Measurement Error Model*

Here, we model the pseudorange rate variance as the sum of the variances of the thermal noise of the PLL and the frequency error of the rover clock:

$$\sigma_{\dot{\rho}}^2 = \sigma_{\text{PLL, vel}}^2 + \sigma_{\text{clock}}^2 \tag{13}$$

This variance is used to model the pseudorange rate measurement error term, which is used to generate the observed pseudorange rate measurements as described in Equation (2). The total measurement error is defined as follows:

$$\sigma_{\text{tot}}^2 = \sigma_{\text{eph, vel}}^2 + \sigma_{\dot{\rho}}^2 \tag{14}$$

Equation (14) is used for a weighting matrix in the measurement filtering to prioritize the measurements with less variance. The implementation of Equation (14) is described in Section 3.

3 | STATE ESTIMATION FRAMEWORK

We now describe the state estimation framework implemented to resolve the rover state with Doppler observables from the Lunar Pathfinder communication signal. In a traditional scenario for localizing a ground user via satellites, an extended Kalman filter (EKF) is commonly used as the nonlinear state estimation framework because it updates the rover's state estimate with each time step, making it a computationally efficient state estimation algorithm. However, in our single-satellite scenario, we can only obtain one measurement at each time step, necessitating the accumulation of these measurements over time. Therefore, for our state estimation framework, we consider a weighted batch filter because it can process multiple measurements over time, drastically improving our measurement geometry in comparison to the EKF. In this section, we detail the formulation of the weighted batch filter for processing pseudorange rate measurements over time while accounting for clock drift.

3.1 | Weighted Batch Filter Formulation

The weighted batch filter aims to refine the rover's state estimate $\hat{\mathbf{x}}$ over time. In this formulation, we define the first three elements of the state estimate $\hat{\mathbf{x}}$ as the rover's position estimate, denoted as $\hat{\mathbf{x}}_p$, as follows:

$$\hat{\mathbf{x}}_p = \begin{bmatrix} x & y & z \end{bmatrix}^\top \tag{15}$$

$$\hat{\mathbf{x}} = \begin{bmatrix} \hat{\mathbf{x}}_p^\top & c \cdot \dot{\delta t} \end{bmatrix}^\top \tag{16}$$

The weighted batch filter first accumulates observed pseudorange rate measurements over time to diversify the measurement geometry. With each iteration k of the batch filter, the batch of measurements processed by the filter increases in size because we retain all previous measurements in this framework. Let us define $\mathbf{y}$ as the stack of N measurements in a given batch of measurements that are accumulated over time:

$$\mathbf{y} = \begin{bmatrix} \dot{\rho}_{\text{obs},1} & \dot{\rho}_{\text{obs},2} & \cdots & \dot{\rho}_{\text{obs},N} \end{bmatrix}^\top \tag{17}$$

For each batch of measurements, we predict the pseudorange rate observables that the rover expects to obtain at time t, given that the rover will have noisy satellite knowledge. The expected pseudorange rate observables $\hat{\dot{\rho}}_{\text{obs}}$ are defined in Equation (18):

$$\hat{\dot{\rho}}_{\text{obs}}^{(t)} = \mathbf{v}_{\mathbf{sat,noise}}^{(t)} \cdot \frac{\mathbf{x}_{\mathbf{sat,noise}}^{(t)} - \hat{\mathbf{x}}_p}{\left\| \mathbf{x}_{\mathbf{sat,noise}}^{(t)} - \hat{\mathbf{x}}_p \right\|} + c\left(\dot{\delta t}_{\text{sat}} - \dot{\delta t}_{\text{rov}} \right) \tag{18}$$

Note that the expected pseudorange rate has a form similar to that of the observed pseudorange rate shown in Equation (2). The expected measurements incorporate the rover's state estimate and the noisy satellite's state, whereas the observed pseudorange rate accounts for the true rover and satellite states along with measurement errors. We set the satellite clock drift $\dot{\delta t}_{\text{sat}}$ to be zero because we assume that the clock onboard the Lunar Pathfinder is stable, as discussed in Section 2.1. The stack of expected measurements $\hat{\dot{\rho}}_{\text{obs}}$ for each filter iteration k is defined as $\hat{\mathbf{y}}_k$.

To refine the rover's state estimate to $\hat{\mathbf{x}}_{k+1}$, we must also refine the batch of expected pseudorange rate measurements to $\hat{\mathbf{y}}_{k+1}$. The expected pseudorange rate model as defined in Equation (18) is nonlinear; thus, we obtain $\hat{\mathbf{y}}_{k+1}$ by applying a first-order Taylor series approximation about the rover's current state estimate $\hat{\mathbf{x}}_k$:

$$\hat{\mathbf{y}}_{k+1} = \hat{\mathbf{y}}_k + \frac{\partial \hat{\mathbf{y}}_k}{\partial \hat{\mathbf{x}}_k}\left(\hat{\mathbf{x}}_{k+1} - \hat{\mathbf{x}}_k \right) \tag{19}$$

$$= \hat{\mathbf{y}}_k + \mathbf{H}_k \delta x \tag{20}$$

Above, we define $\delta\mathbf{x}$ as the difference in the current and updated rover state estimate. The first derivative of the expected pseudorange rate measurement stack $\hat{\mathbf{y}}_k$ with respect to the current rover state estimate $\hat{\mathbf{x}}_k$ is defined as the measurement Jacobian matrix $\mathbf{H}_k$:

$$\mathbf{H}_k = \begin{bmatrix} \frac{\partial \hat{\dot{\rho}}_{\text{obs},1}}{\partial \hat{\mathbf{x}}_k} & \frac{\partial \hat{\dot{\rho}}_{\text{obs},2}}{\partial \hat{\mathbf{x}}_k} & \cdots & \frac{\partial \hat{\dot{\rho}}_{\text{obs},N}}{\partial \hat{\mathbf{x}}_k} \end{bmatrix}^\top \in \mathbb{R}^{N \times 4} \tag{21}$$

$$\frac{\partial \hat{\dot{\rho}}_{\text{obs},t}}{\partial \hat{\mathbf{x}}_k} = \begin{bmatrix} \frac{\partial \hat{\dot{\rho}}_{\text{obs},t}}{\partial x_k} & \frac{\partial \hat{\dot{\rho}}_{\text{obs},t}}{\partial y_k} & \frac{\partial \hat{\dot{\rho}}_{\text{obs},t}}{\partial z_k} & 1 \end{bmatrix} \tag{22}$$

When refining the rover's state estimate, we must take into account the rover clock drift, as it contributes to the rover's expected pseudorange rate measurements. Therefore, in the measurement Jacobian, we consider the rover clock drift (multiplied by the speed of light) as the fourth element of the rover state. Recall that we assume that the rover clock drift is constant throughout the measurement window; thus, the fourth column of the Jacobian is $\mathbf{1}_{N\times 1}$.

Ultimately, the rover's updated state estimate $\hat{\mathbf{x}}_{k+1}$ is obtained by minimizing the difference between the observed pseudorange rate measurements and the expected pseudorange rate measurements that we have refined, as shown in Equation (23). We define this difference as the measurement residual $\delta\mathbf{y}$. With the Taylor series approximation from Equation (20), the cost function to minimize is shown in Equation (24), which has a closed-form solution, as shown in Equation (25):

$$J = \left\| \mathbf{y} - \hat{\mathbf{y}}_{k+1} \right\|_{\mathbf{W}}^2 \tag{23}$$

$$= \left\| \delta\mathbf{y} - \mathbf{H}_k \delta\mathbf{x} \right\|_{\mathbf{W}}^2 \tag{24}$$

$$\delta\mathbf{x} = \left(\mathbf{H}_k^\top \mathbf{W} \mathbf{H}_k \right)^{-1} \mathbf{H}_k^\top \mathbf{W} \delta\mathbf{y} \tag{25}$$

We use a weighting matrix $\mathbf{W}$ in the measurement filtering to prioritize the measurements with less variance. The weighting matrix $\mathbf{W}$ is a function of the total measurement error, as defined in Equation (14):

$$\mathbf{W} = \mathrm{diag}\left(\sigma_{\mathrm{tot},1}^{-2}, \ldots, \sigma_{\mathrm{tot},N}^{-2} \right) \tag{26}$$

For each batch of measurements, we iteratively update $\delta\mathbf{x}$ (and thus $\hat{\mathbf{x}}$) until $\delta\mathbf{x}$ is negligibly small. This iterative process, the Gauss–Newton method, is outlined in Algorithm 1. The `predict_pseudorange_rate` function in Algorithm 1 outputs the expected measurement stack and the Jacobian, as defined in Equations (18) and (21), respectively. The updated state estimate is stored after each batch is processed. With each new batch of measurements, the rover's state estimate is re-initialized and refined once again through the batch filter. When the satellite is not visible to the rover, measurements cannot be collected. During this occultation period, the rover's current state estimate is not updated.

3.2 | Filter Initialization

We modify the initialization of the Gauss–Newton method by embedding prior knowledge about the rover's initial position estimate $\hat{\mathbf{x}}_{p,0}$ in the algorithm. In other words, we augment $\mathbf{H}_k$ and $\delta\mathbf{y}$ by treating the residual between the initial position estimate $\hat{\mathbf{x}}_{p,0}$ and the current position estimate $\hat{\mathbf{x}}_{p,k}$ as a measurement. The uncertainty of the initial position estimate is also embedded in the weighting matrix $\mathbf{W}$. The augmentations to $\mathbf{H}_k$, $\delta\mathbf{y}$, and $\mathbf{W}$ can be found in lines 5, 6, and 7 of Algorithm 1, respectively.

This modification ensures that there is no significant divergence from the rover's true state early in the simulation. When the initial position estimate is not embedded into the algorithm, we observe a spike in the rover's positioning error. This augmentation helps maintain a stable estimate until there are enough measurements to resolve the rover's state at a finer accuracy.

ALGORITHM 1
Weighted Gauss–Newton Method for Rover Localization

Require: Initial rover state estimate $\hat{\mathbf{x}}_0$, observed pseudorange rate measurements $\mathbf{y}$, rover's knowledge of satellite position $\mathbf{x}_{\mathbf{sat,noise}}$ and velocity $\mathbf{v}_{\mathbf{sat,noise}}$, measurement time t

Ensure: Final rover state estimate $\hat{\mathbf{x}}$

for each batch of measurements at time t **do**
  if satellite is visible **then**
    while $||\delta\mathbf{x}|| > 10^{-9}$ **do**
      $[\hat{\mathbf{y}}_k, \mathbf{H}_k] \leftarrow$ `predict_pseudorange_rate`$(\mathbf{x}_{\mathbf{sat,noise}}, \mathbf{v}_{\mathbf{sat,noise}}, \hat{\mathbf{x}})$
      $\mathbf{H}_k \leftarrow [\mathbf{I}_{3\times3}, \mathbf{0}_{3\times1}; \mathbf{H}_k]$
      $\delta\mathbf{y} \leftarrow [\hat{\mathbf{x}}_{p,0} - \hat{\mathbf{x}}_p; \mathbf{y} - \hat{\mathbf{y}}_k]$
      $\mathbf{W} \leftarrow \text{diag}\left(\sigma_{\text{pos}}^{-2}, \sigma_{\text{pos}}^{-2}, \sigma_{\text{pos}}^{-2}, \sigma_{\text{tot},1}^{-2}, \ldots, \sigma_{\text{tot,N}}^{-2}\right)$
      $\delta\mathbf{x} \leftarrow \left(\mathbf{H}_k^T\mathbf{W}\mathbf{H}_k\right)^{-1}\mathbf{H}_k^T\mathbf{W}\delta\mathbf{y}$
      $\hat{\mathbf{x}} \leftarrow \hat{\mathbf{x}} + \delta\mathbf{x}$
    end while
  end if
end for
return $\hat{\mathbf{x}}$

4 | SIMULATION SET-UP

In this section, we outline the simulation set-up used to evaluate the feasibility and performance of single-satellite lunar surface state estimation with only Doppler shift observables. We discuss the location of the rover on the Moon where state estimation is performed, as well as the simulation parameters for the Monte Carlo simulations.

4.1 | Initialized Rover Position

According to the Endurance Mission Concept Study Report (Keane et al., 2022), two implementation options are being considered for the Endurance mission: (1) Endurance-R, where the rover will rendezvous with an Earth return vehicle to return the samples and (2) Endurance-A, where the rover will meet with the Artemis astronauts, who will then bring the samples back to Earth. Endurance-R will begin its path at the Poincaré Q basin and end at the Apollo peak ring, whereas Endurance-A will start in the central SPA basin and reunite with the astronauts at the Artemis Basecamp. For this study, we have selected three key locations–Poincaré Q, the Apollo peak ring, and the Artemis Basecamp–as shown in Figure 2, because these locations are sufficiently spatially distributed with respect to each other in the SPA basin. Cortinovis et al. (2024) also conducted their analyses at these locations. Table 5 details the latitude and longitude coordinates of the selected waypoints.

Upon landing on the surface of the Moon, the rover will have good initial state estimation knowledge via manual human-in-the-loop map comparison. Therefore, the initial positioning error is on the order of 100 m for this study. The initial state estimate is randomly sampled from a Gaussian normal distribution such that $\hat{\mathbf{x}}_0 \sim \mathcal{N}(\mathbf{0}, \text{diag}[100^2, 100^2, 100^2])$ m.

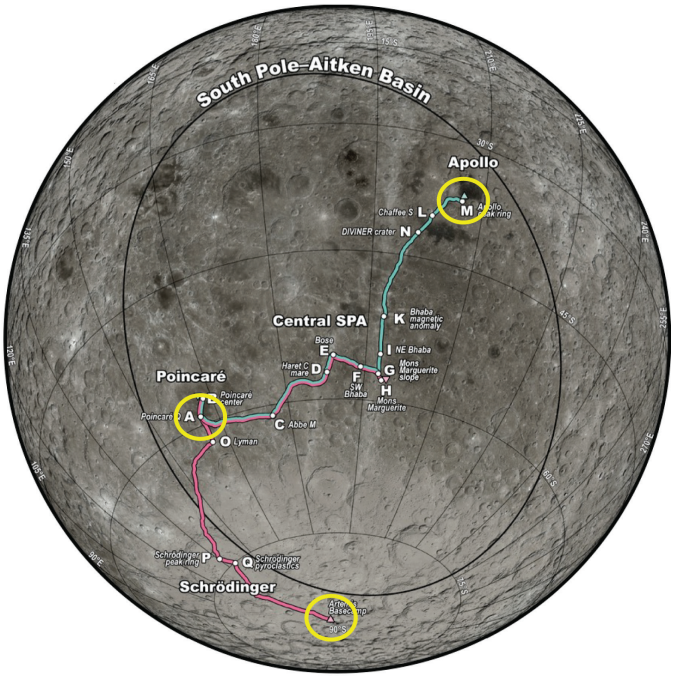

FIGURE 2 Map of Endurance's proposed path with chosen waypoints circled in yellow; figure adapted from Keane et al. (2022)

TABLE 5
Latitude and Longitude of the Selected Waypoints
Keane et al. (2022) specified the coordinates for Poincaré Q and the Apollo peak ring. Because the exact location of the Artemis Basecamp is not yet finalized, we have approximated its location to be at the South Pole.

Location	Latitude [°]	Longitude [°]
Poincaré Q	−59.12448	161.05104
Apollo peak ring	−37.7115	−153.0430
Artemis Basecamp	−90	0

4.2 | Simulation Parameters

The starting epoch to determine the Lunar Pathfinder's orbit with respect to the Moon is set to 2030 October 1, 00:00 UTC. We consider two orbital periods, or approximately 22 h, for our simulation time unless otherwise specified. Measurements are sampled at 1 Hz, and the batch filter provides a new update of the rover state every 180 s. Note that no measurements are acquired when the Lunar Pathfinder satellite is not visible to the rover. Metrics that define signal availability are described in Section 5.1. Because we perform random sampling of the initial position estimate, satellite ephemeris errors, and Doppler measurement errors, we conduct 100 Monte Carlo realizations of the batch filter per location of interest.

5 | ANALYSIS AND RESULTS

In this section, we first discuss the availability of the communication signal at each location considered. Then, we address the performance of the state estimation framework at each location with nominal error modeling. In this study, we

investigate the time for the absolute positioning error to converge to below 10 m, which is the global localization error requirement for the Endurance mission (Cauligi et al., 2023). The absolute positioning error of the rover is defined as the L_2 norm of the difference between the true and the estimated position. We consider the mean and the 99th percentile of the absolute positioning error across 100 Monte Carlo realizations as our performance metrics. Empirical analysis indicates that 100 Monte Carlo runs are sufficient to stabilize these metrics, while maintaining computational efficiency. Finally, we discuss the effects of different degrees of clock stability and satellite ephemeris errors on achieving the desired state estimation accuracy.

5.1 | Signal Availability

The design of the Lunar Pathfinder's ELFO allows for favorable coverage of the SPA region. Figure 3 presents the received C/N_0 and the elevation mask over two orbital periods. Contrary to intuition, the received C/N_0 is highest when the satellite is at its maximum elevation (i.e., when the satellite is farthest from the rover). We would expect C/N_0 to reach a minimum at the highest elevation point owing to the increased free-space path loss. However, this assumption only holds if the satellite antenna is actively tracking the rover. In our simulations, we assume that the Lunar Pathfinder provides services to multiple lunar assets; thus, its transmitting antenna is always pointing in the nadir direction rather than adjusting to individual users. As a result, the directionality of the transmitting antenna significantly influences the received C/N_0. When the satellite is directly overhead, it points most accurately toward the rover, leading to a higher C/N_0 despite the larger distance.

We consider an elevation mask of 5° for satellite visibility, and we define the signal as available when the received signal strength is larger than 30 dB Hz (as defined by Nardin et al. (2023) and Melman et al. (2022)). Based on the respective thresholds, the 5° elevation mask is the limiting factor for satellite visibility in comparison to the signal strength threshold of 30 dB Hz. The regions in which the satellite is not visible to the rover are shown as gray occultation zones in later figures.

Table 6 presents the total time duration for which the satellite signal is unavailable, either because of an insufficient received C/N_0 or a lack of satellite visibility.

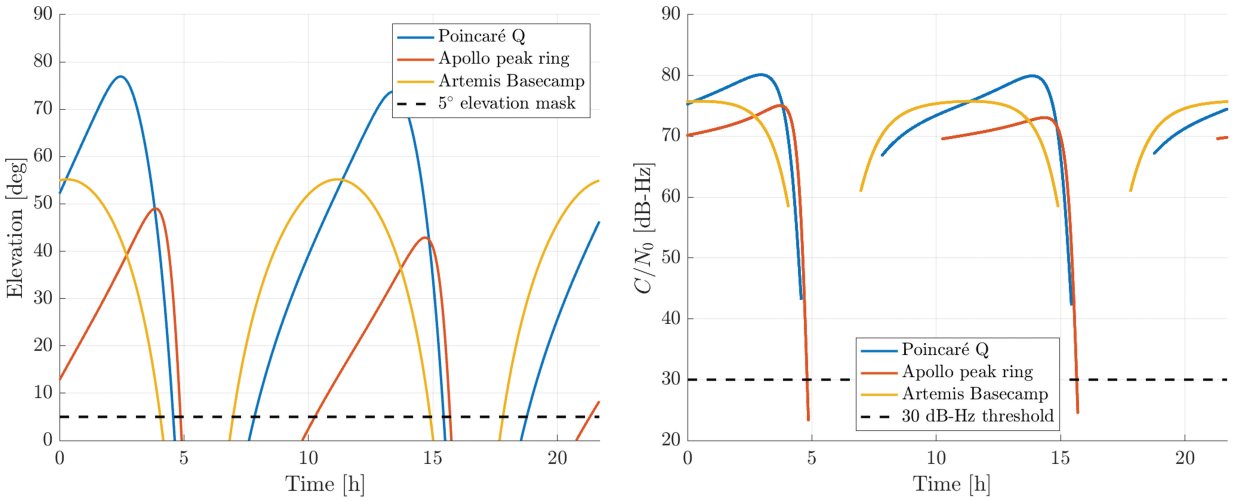

FIGURE 3 [Left] Elevation angle of the Lunar Pathfinder and [right] received carrier-to-noise density ratio C/N_0 (given that the satellite is visible) over two orbital periods for each of the three lunar sites considered

TABLE 6
Length of Time, in Hours, When the Elevation Mask is Less Than 5° and the Received C/N_0 is Less Than 30 dB Hz (Given That the Satellite is Visible) for Each Key Location
The total length of the occultation period, considering both metrics, is also provided. Each cell displays the length of time of the occultation period corresponding to the first and second orbits.

Location	Length of the first and second occultation periods					
	Elevation < 5°		C/N_0 < 30 dB Hz		Total	
	First	Second	First	Second	First	Second
Poincaré Q	3.28 h	3.36	0.00 h	0.00 h	3.28 h	3.36 h
Apollo peak ring	5.41 h	5.63 h	0.05 h	0.05 h	5.46 h	5.68 h
Artemis Basecamp	2.92 h	2.92 h	0.00 h	0.00 h	2.92 h	2.92 h

The total occultation period for each location is the union of the two metrics (i.e., when C/N_0 is less than 30 dB Hz or when the elevation mask is less than 5°). The Artemis Basecamp location has the shortest occultation period while the Apollo peak ring has the longest occultation period, owing to the elevation mask. Because the Artemis Basecamp is located exactly at the South Pole, the rover position is symmetric relative to the Lunar Pathfinder, as shown in the elevation plot in Figure 3. Owing to this symmetry, there is no change in the occultation period between the first and second orbits for the Artemis Basecamp location. In contrast, for the Poincaré Q and Apollo peak ring locations, the occultation periods increase slightly between the first and second orbits because of the satellite's relative motion.

Cortinovis et al. (2024) also used the same metrics for signal availability. However, because those authors assumed that the satellite is equipped with a navigation payload, they modeled their transmitter antenna according to the Lunar Communications Relay and Navigation Systems (LCRNS) requirements, resulting in smaller C/N_0 values than we observe with the transmitter parameters used in this study. Thus, our modeling of a lunar satellite with a communication antenna results in longer periods of signal availability in comparison to a lunar satellite with a navigation antenna (Cortinovis et al., 2024).

Figure 4 illustrates the behavior of the Doppler shift measurements. Positive Doppler measurements signify that the Lunar Pathfinder is approaching its peak elevation over the stationary Endurance rover, and negative measurements indicate that the satellite is receding. In the right panel, the Lunar Pathfinder is traversing its path in the clockwise direction. The blue point in the figure marks the point in the satellite's path at which the mean anomaly is 180°. At time $t = 0$ in the left panel, the satellite is at the blue point in the right panel. When the satellite recedes away from the blue point, we observe a negative Doppler shift until the satellite enters the first occultation zone. Once the satellite re-enters the rover's line of sight, the satellite approaches its peak elevation, resulting in a positive Doppler shift until a zero Doppler shift is reached at the blue point.

For our state estimation experiments, we begin measurement collection once the satellite is visible to the rover (as indicated by the black arrow in Figures 4 and 5) to maximize the time for the rover to refine its position estimate before hitting an occultation zone. The visible and non-visible parts of the Lunar Pathfinder orbit with respect to the rover are shown in the right panel of Figure 4 for when the rover is located at the Artemis Basecamp. Corresponding results for when the rover is located at Poincaré Q and the Apollo peak ring are shown in Figure 5. We observe that the satellite enters longer occultation periods when the rover is located in higher-latitude regions such as the Apollo peak ring.

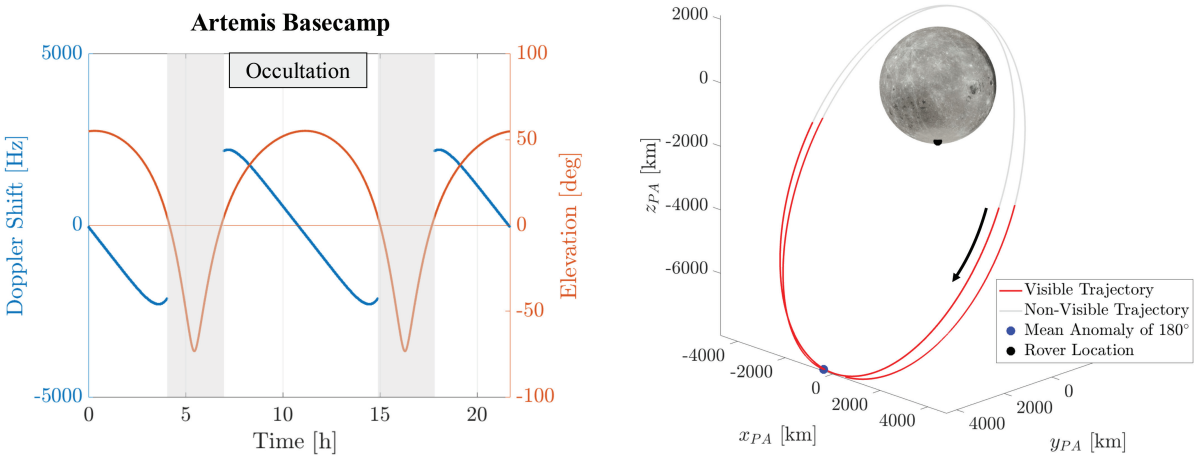

FIGURE 4 [Left] Doppler shift and elevation and [right] trajectory of the Lunar Pathfinder over two orbital periods
The rover location is set to be at the Artemis Basecamp. Time $t = 0$ in the left panel corresponds to the time when the satellite is located at the blue point in the right panel. Measurement collection for state estimation begins once the satellite is visible to the rover, as shown by the black arrow.

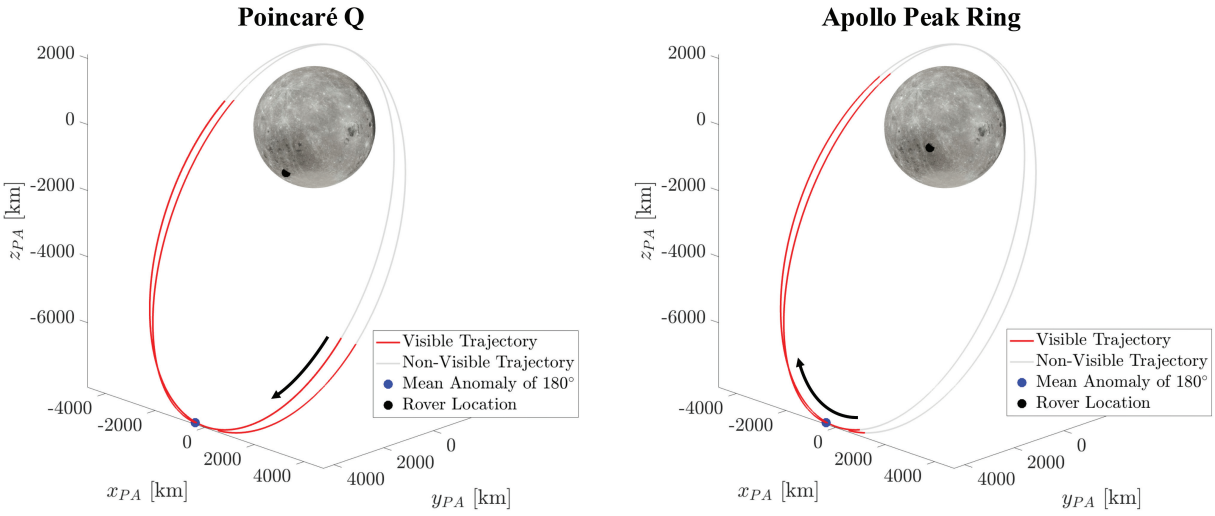

FIGURE 5 Visible and non-visible parts of the Lunar Pathfinder orbit when the rover is located at [left] Poincaré Q and [right] the Apollo peak ring
The black arrow denotes the start of measurement collection for filtering. We observe longer occultation periods for higher-latitude locations.

5.2 | State Estimation Performance

Using the weighted batch filter framework, we refine the rover's position estimate over time for each of the three locations. The mean μ, range of 1σ values, and 99% error of the position estimation for 100 Monte Carlo realizations are shown in Figure 6. The figure also shows the occultation zones and the 10-m threshold for each location. All three plots are simulated under the assumption that the rover is equipped with an SRS PRS 10 clock and that the ephemeris errors are 4.48 m in position and 0.40 mm/s in velocity (the justification for this ephemeris error is described in Section 5.4). Table 7 summarizes the time required for the mean μ and the 99% error of 100 Monte Carlo realizations to achieve sub-10-m accuracy.

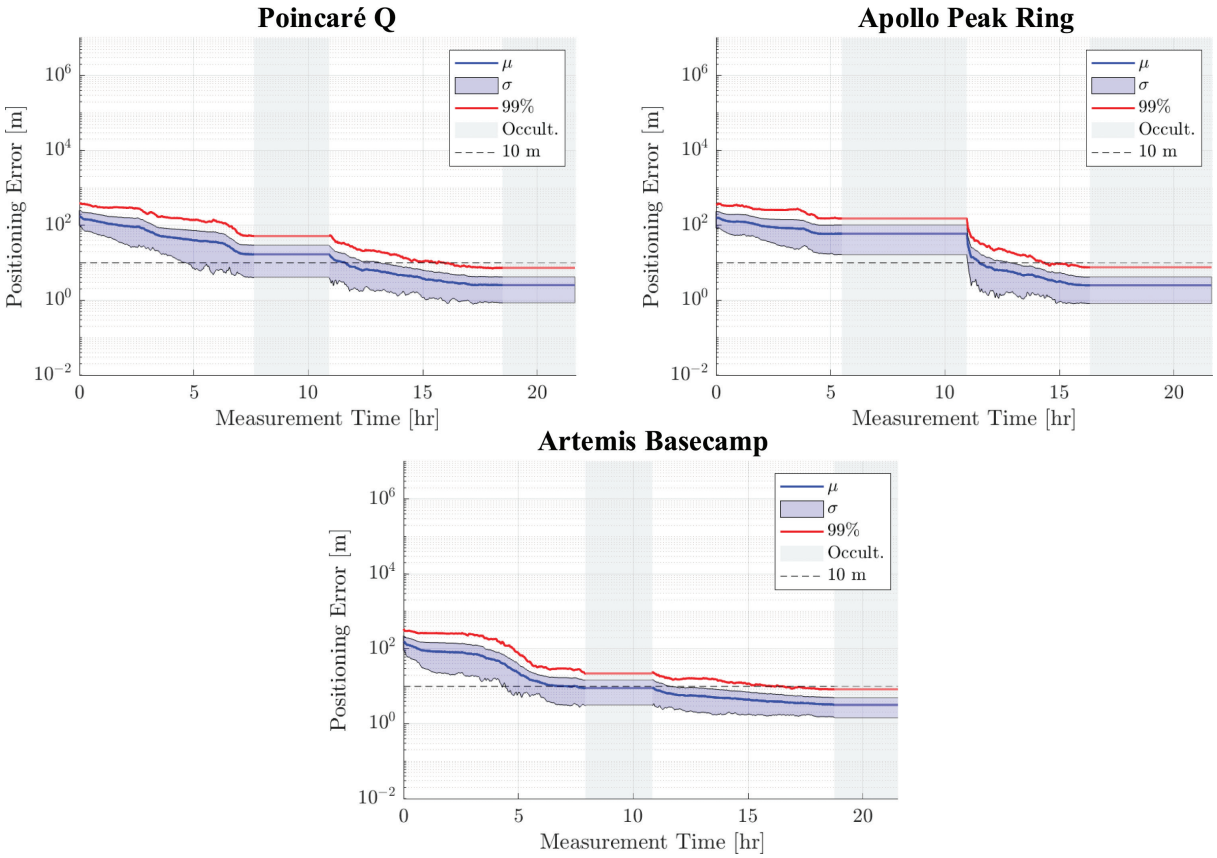

FIGURE 6 Positioning error over two orbital periods at three different locations
These plots are simulated with satellite ephemeris errors based on the LCRNS's SISE specification and with the assumption that the rover is equipped with an SRS PRS 10 clock.

TABLE 7
Time, in Hours, for the Mean and 99% Error of 100 Monte Carlo Runs to Converge Below the 10-m Threshold for Each Location
We assume that the rover is equipped with an SRS PRS 10 clock and that the satellite ephemeris errors align with that of the LCRNS's SISE specification.

Location	Time to reach ≤ 10 m	
	Mean [h]	99% error [h]
Poincaré Q	11.6	16.0
Apollo peak ring	11.5	14.4
Artemis Basecamp	7.5	16.4

From Figure 6, we observe that the mean position error μ reaches sub-10-m-level accuracy within the first 12 h for the Poincaré Q and Apollo peak ring locations and within 8 h for the Artemis Basecamp location. The 99% error converges to 10 m within the first two orbital periods for all three locations. The mean positioning error for the Artemis Basecamp location is the only metric that is able to converge to below 10 m before the first occultation period. For an autonomous rover such as Endurance, the mean contact time per day during which the Lunar Pathfinder will be providing communication services is 529 min, or 8.82 h (SSTL, 2022). While the exact periods of time during which the Lunar Pathfinder will provide communication services have not yet been specified, according to our analysis, we find that the rover, on average, will be able to localize itself within the desired accuracy within 8.82 h only when the rover is located in the more southern regions of the

rover's path. Otherwise, the rover will require a larger measurement window to successfully localize.

Despite having the shortest occultation period, the Artemis Basecamp location resulted in the largest 99% positioning error convergence time in comparison to the other locations, as shown in Table 7. Because the Artemis Basecamp is located exactly at the South Pole, the diversity of measurements between the first visibility zone to the second visibility zone is minimal. Therefore, the rover's state estimate is slow to improve after the first occultation zone when the rover is located at the Artemis Basecamp.

Overall, we observe a plateau in positioning error in the first 3–4 h for all three locations. This plateauing behavior occurs because we embed prior knowledge about the rover's initial position estimate, as described in Section 3.2. During the first few hours, the rover does not have sufficient measurement diversity to refine the rover's state estimate to a finer accuracy. We find that the 99% error in this study takes approximately 10.7–13.6 h longer to converge than in a previous study using two-way ranging measurements with a weighted batch filter (Cortinovis et al., 2024). The convergence window of the 99% error in this study includes an entire occultation period, which adds an additional 2.92–5.68 h during which the estimate is not being refined. However, it is essential to note that a comprehensive comparison of this study and that of Cortinovis et al. (2024) is limited by the differences in modeling the measurement and ephemeris errors. Furthermore, we take into account noise due to the rover's onboard clock, which is not assessed in the study of Cortinovis et al. (2024), as their model utilized two-way measurements.

5.3 | Sensitivity Study on Clock Stability

NASA has not yet specified the type of clock that the Endurance rover will carry onboard. To help inform this decision, we conducted a sensitivity study to evaluate various clock candidates for the specific use case of rover localization. Table 4 details the SWaPs, TDEVs per day, and PSD coefficients for the four rover clock candidates we consider in this study. We evaluated the time to achieve sub-10-m accuracy for each of the rover clocks and have summarized the performance metrics in Table 8.

We prioritize minimizing weight and power consumption of the rover's onboard clock, owing to the high cost of deploying heavy equipment to the Moon and the significant power demands of the rover's 2000-km traverse. Therefore, we conduct a trade-off analysis between clock stability and these two metrics. Figure 7 displays a plot of the mean convergence time to achieve sub-10-m accuracy for the clock candidates, with the weights and power consumptions plotted on the y-axis. As expected, the heavier and higher-power-consuming clocks (which correlate to less clock drift) have a shorter time to convergence in comparison to the lower-SWaP clocks. The smallest clock that we consider–the Microchip chip-scale atomic clock (CSAC)–requires five orbital periods for the mean time to converge. The 99% error is unable to converge within six orbital periods for the Microchip CSAC. Therefore, we do not recommend the Microchip CSAC for single-satellite localization.

The most stable clock–the Excelitas rubidium atomic frequency standard (RAFS)–is able to converge in 4.9 h. If clock weight (or power consumption) and performance time both need to be minimized with equal magnitude, we recommend the SRS PRS 10 and the Microchip miniature atomic clock (MAC) for the Endurance rover, as they have a mass of less than 1 kg, require less than 15 W

TABLE 8
Time, in Hours, for the Mean and 99% Error of 100 Monte Carlo Runs to Converge Below the 10-m Threshold for Each of the Different Clock Types (Listed in Order of Increasing SWaP)
The rover is located at the Artemis Basecamp for these simulations, and we use the LCRNS's SISE values to describe its ephemeris knowledge.

Clock type	Time to reach ≤ 10 m	
	Mean [h]	99% error [h]
Microchip CSAC	50.1	Did not converge within 65 h
Microchip MAC	11.2	26.7
SRS PRS 10	7.5	16.4
Excelitas RAFS	4.9	11.1

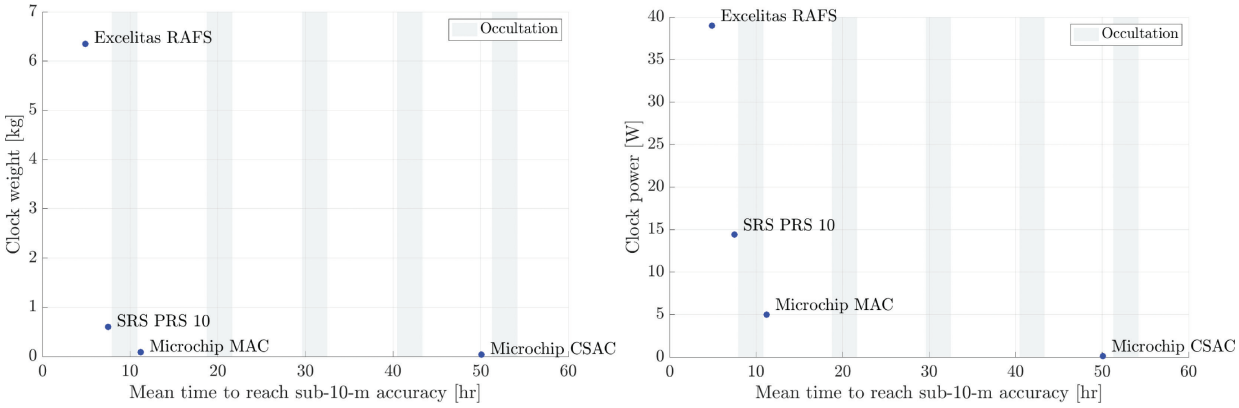

FIGURE 7 Mean time to reach sub-10-m accuracy for the four clock candidates, with their respective [left] clock weights and [right] clock power consumptions plotted on the *y*-axis
This study was performed under the assumption that the rover is located at the Artemis Basecamp and is using the LCRNS's SISE values to describe its ephemeris knowledge.

for operation, and converge within 1–2 orbital periods. However, if rapid localization is more critical than additional weight on the rover, we recommend the Excelitas RAFS.

5.4 | Sensitivity Study on Satellite Ephemeris Errors

Because of the uncertainty of the Lunar Pathfinder's ephemeris knowledge, we examine the effects of varying degrees of satellite ephemeris errors on achieving the desired position estimation accuracy. We consider the lowest satellite ephemeris errors to be those cited in the Lunar Relay Services Requirements Document for lunar navigation satellites, which are $\sigma_{\text{eph,pos}} = 4.48$ m and $\sigma_{\text{eph,vel}} = 0.40$ mm/s (NASA, 2022a). For our sensitivity analysis, we linearly inflate ephemeris errors ranging from 10.00 to 50.00 m in position and from 1.00 to 5.00 mm/s in velocity, as shown in Figure 8.

We observe that the positioning error converges to below the 10-m threshold in roughly the same amount of time for the lowest ephemeris errors and for $\sigma_{\text{eph,pos}} = 10.00$ m and $\sigma_{\text{eph,vel}} = 1.00$ mm/s. However, for larger ephemeris errors, the 99% positioning error is unable to converge within two orbital periods, resulting in an additional 2.92 h for the time to convergence. Based on this sensitivity study, we recommend that the Lunar Pathfinder's ephemeris errors remain below 20.00 m in position and 2.00 mm/s in velocity.

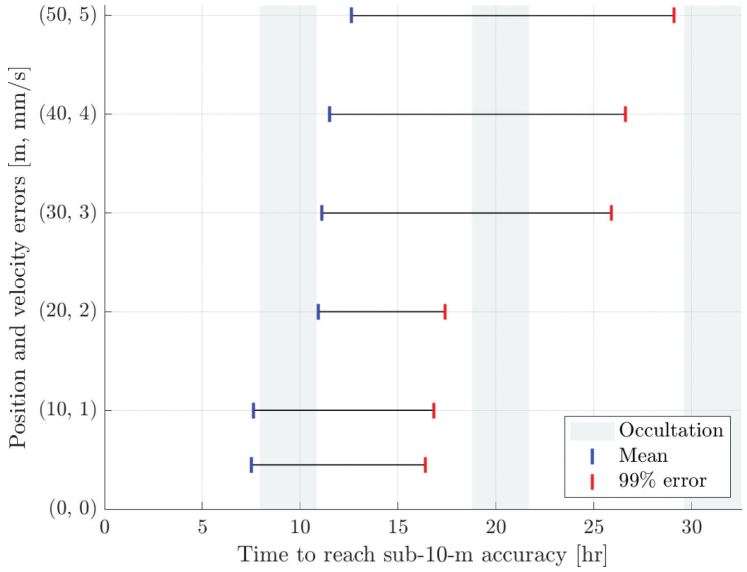

FIGURE 8 Time for the mean and 99th percentile of Monte Carlo runs to converge to below 10 m for different ephemeris errors in position [m] and velocity [mm/s]
This study assumes that the rover is located at the Artemis Basecamp and is equipped with an SRS PRS 10 clock.

6 | CONCLUSIONS

We have presented a localization framework for the NASA Endurance rover using only the downlink communication signals from a single satellite, the Lunar Pathfinder, with no navigation payload. We designed a weighted batch filter framework that accumulates Doppler shift measurements and refines the position estimate of the stationary rover. For our analysis, we formulated a Doppler measurement model to simulate realistic measurement errors from the Lunar Pathfinder's communication signal, which accounts for the rover clock drift, satellite ephemeris errors, and carrier tracking loop errors. We further modeled the signal link budget from the Lunar Pathfinder satellite to the Endurance rover while incorporating models of the satellite and receiver antennae, according to the available specifications of the respective missions. Through our analysis, we found that the mean and 99% positioning error of 100 Monte Carlo realizations were able to localize the rover with the desired sub-10-m accuracy within two orbital periods. We also performed sensitivity studies on the rover's clock type and ephemeris knowledge to better inform design decisions for the rover. Through this study, we demonstrated that utilizing opportunistic Doppler shift measurements as the only navigation observable is a feasible localization framework for the Endurance mission. Future efforts may include comparing the state estimation performance when using two satellites for localization and investigating the scenario in which the Endurance rover is moving during the measurement window.

ACKNOWLEDGMENTS

This research was supported by a National Science Foundation Graduate Research Fellowship (No. DGE-2146755) and a Stanford Knight-Hennessy Scholars graduate fellowship. We would like to acknowledge Keidai Iiyama for insightful discussions. We would also like to thank the other members of the Stanford Navigation and Autonomous Vehicles Laboratory for their helpful feedback and support.

REFERENCES

Audet, Y., Melman, F. T., Molli, S., Sesta, A., Plumaris, M., Psychas, D., Swinden, R., Girodano, P., & Ventura-Traveset, J. (2024). Positioning of a lunar surface rover on the South Pole using LCNS and DEMs. *Advances in Space Research, 74*(6), 2532–2550. https://doi.org/10.1016/j.asr.2024.06.022

Bhamidipati, S., Mina, T., & Gao, G. (2023). A case study analysis for designing a lunar navigation satellite system with time-transfer from Earth-GPS. *NAVIGATION, 70*(4). https://doi.org/10.33012/navi.599

Borio, D., Sokolova, N., & Lachapelle, G. (2011). Doppler measurement accuracy in standard and high-sensitivity global navigation satellite system receivers. *IET Radar, Sonar and Navigation*, *5*(6), 657–665. https://doi.org/10.1049/iet-rsn.2010.0249

Cauligi, A., Swan, R. M., Ono, H., Daftry, S., Elliot, J., Matthies, L., & Atha, D. (2023). ShadowNav: Crater-based localization for nighttime and permanently shadowed region lunar navigation. *Proc. of the 2023 IEEE Aerospace Conference,* Big Sky, MT. https://doi.org/10.1109/AERO55745.2023.10115745

Cheung, K.-M., Lee, C., Jun, W., & Lightsey, G. (2019). Single-satellite Doppler localization with law of cosines (LOC). *Proc. of the 2019 IEEE Aerospace Conference*, Big Sky, MT, 1–12. https://doi.org/10.1109/AERO.2019.8742181

Coimbra, K. M. Y., Cortinovis, M., Mina, T., & Gao, G. (2024). Single-satellite lunar navigation via Doppler shift observables for the NASA Endurance mission. *Proc. of the 37th International Technical Meeting of the Satellite Division of the Institute of Navigation (ION GNSS+ 2024)*, Baltimore, MD, 3250–3265. https://doi.org/10.33012/2024.19939

Cortinovis, M., Mina, T., & Gao, G. (2024). Assessment of single satellite-based lunar positioning for the NASA Endurance mission. *Proc. of the 2024 IEEE Aerospace Conference,* Big Sky, MT. https://doi.org/10.1109/AERO58975.2024.10521264

Daftry, S., Chen, Z., Cheng, Y., Tepsuporn, S., Khattak, S., & Matthies, L. (2023). LunarNav: Crater-based localization for long-range autonomous lunar rover navigation. *Proc. of the 2023 IEEE Aerospace Conference,* Big Sky, MT. https://doi.org/10.1109/AERO55745.2023.10115640

Delépaut, A., Giordano, P., Ventura-Traveset, J., Blonski, D., Schönfeldt, M., Schoonejans, P., Aziz, S., & Walker, R. (2020). Use of GNSS for lunar missions and plans for lunar in-orbit development. *Advances in Space Research*, *66*(12), 2739–2756. https://doi.org/10.1016/j.asr.2020.05.018

Folta, D., Bosanac, N., Elliott, I., Mann, L., Mesarch, R., & Rosales, J. (2022). Astrodynamics convention and modeling reference for lunar, cislunar, and libration point orbits [No. NASA/TP-20220014814]. *NASA, Technical Publication*. https://ntrs.nasa.gov/citations/20220014814

Iiyama, K., Bhamidipati, S., & Gao, G. (2023). Terrestrial GPS time-differenced carrier-phase positioning of lunar surface users. *Proc. of the 2023 IEEE Aerospace Conference,* Big Sky, MT. https://doi.org/10.1109/AERO55745.2023.10115673

Jun, W. W., Cheung, K.-M., & Lightsey, E. G. (2023). Improved surface positioning with measurement differences in joint Doppler and ranging. *Proc. of the 2023 IEEE Aerospace Conference,* Big Sky, MT. https://doi.org/10.1109/AERO55745.2023.10115954

Jun, W. W., Cheung, K.-M., Lightsey, E. G., & Lee, C. (2022). A minimal architecture for real-time lunar surface positioning using joint Doppler and ranging. *IEEE Transactions on Aerospace and Electronic Systems*, *58*(2), 1367–1376. https://doi.org/10.1109/TAES.2021.3122876

Kaplan, E. D., & Hegarty, C. (2017). *Understanding GPS/GNSS: Principles and applications* [ISBN: 9781630814427]. Artech House. https://us.artechhouse.com/Understanding-GPSGNSS-Principles-and-Applications-Third-Edition-P1904.aspx

Keane, J. T., Tikoo, S. M., & Elliot, J. (2022). Endurance: Lunar South Pole-Aitken basin traverse and sample return rover. *NASA Jet Propulsion Laboratory, Technical Report*. https://science.nasa.gov/wp-content/uploads/2023/11/endurance-spa-traverse-and-sample-return.pdf

Kershner, R. B., & Newton, R. R. (1962). The Transit system. *The Journal of Navigation*, *15*(2), 129–144. https://doi.org/10.1017/S0373463300035943

Krawinkel, T., & Schön, S. (2016). Benefits of receiver clock modeling in code-based GNSS navigation. *GPS Solutions*, *20*, 687–701. https://doi.org/10.1007/s10291-015-0480-2

Melman, F. T., Zoccarato, P., Orgel, C., Swinden, R., Giordano, P., & Ventura-Traveset, J. (2022). LCNS positioning of a lunar surface rover using a DEM-based altitude constraint. *Remote Sensing*, *14*(16), 3942. https://doi.org/10.3390/rs14163942

Misra, P., & Enge, P. (2010). *Global Positioning System: Signals, measurements & performance* [ISBN-13: 978-0970954428]. Ganga-Jamuna Press. https://www.navtechgps.com/global-positioning-system-signals-measurements-and-performance-revised-second-edition-paperback/

Nardin, A., Minetto, A., Guzzi, S., Dovis, F., Konitzer, L., & Parker, J. J. K. (2023). Snapshot tracking of GNSS signals in space: A case study at lunar distances. *Proc. of the 36th International Technical Meeting of the Satellite Division of the Institute of Navigation (ION GNSS+ 2023)*, Denver, CO, 3267–3281. https://doi.org/10.33012/2023.19174

NASA. (2022a). Lunar communications relay and navigation systems (LCRNS) lunar relay services requirements document (SRD) [ESC-LCRNS-REQ-0090, Revision B w/DCN 001].

NASA Goddard Space Flight Center, Technical Report. https://esc.gsfc.nasa.gov/static-files/ESC-LCRNS-REQ-0090%20Rev_B%2012-05-2022%20DCN001.pdf

NASA. (2022b). NASA's lunar exploration program overview. *NASA, Technical Report*. https://www.nasa.gov/wp-content/uploads/2020/12/artemis_plan-20200921.pdf

O'Dea, A., Kinman, P., Pham, T. T., & Chang, C. (2019). Doppler tracking [DSN No. 810-005, 202, Rev. C]. *Deep Space Network*. https://deepspace.jpl.nasa.gov/dsndocs/810-005/202/202C.pdf

Psiaki, M. L. (2021). Navigation using carrier Doppler shift from a LEO constellation: TRANSIT on steroids. *NAVIGATION*, *68*(3), 621–641. https://doi.org/10.1002/navi.438

Schmittberger, B. L., & Scherer, D. R. (2020). *A review of contemporary atomic frequency standards.* arXiv. https://doi.org/10.48550/arXiv.2004.09987

Surrey Satellite Technology Ltd. (2022). Lunar Pathfinder: Data relay satellite in orbit around the Moon [Service Guide (V4)]. *SSTL*. https://www.sstl.co.uk/getmedia/9efe3cc5-6b5b-4fd1-bbd7-443bc2d21848/Lunar-Pathfinder-Service-Guide-V004.pdf

How to cite this article: Coimbra, K. M. Y., Cortinovis, M., Mina, T., & Gao, G. (2025). Single-satellite lunar navigation via Doppler shift observables for the NASA Endurance mission. *NAVIGATION*, *72*(3). https://doi.org/10.33012/navi.710